High Resolution Isotropic 3D CAIPIRINHA SPACE MRI of the Musculoskeletal System

Gaurav K. Thawait, M.D.; Rushyuan J. Lee, M.D.; Derek F. Papp, M.D.; Jan Fritz, M.D.

Johns Hopkins University School of Medicine, Baltimore, MD, USA

Introduction

Magnetic resonance imaging (MRI) has an important role in the diagnosis, characterization and surveillance of many conditions affecting the musculoskeletal system, including trauma, degeneration, inflammation and infection of bone, joints, ligaments, tendons, and muscles.

The high-contrast resolution of native and contrast-enhanced MRI enables multiparameteric characterization of a multitude of conditions. The morphological analysis of musculoskeletal structures and fine detail are crucial for the detection and characterization of abnormalities, such as ligamentous tears, cartilage defects, muscle-tendon unit injuries, fractures as well as bone marrow abnormalities, collections, and neoplastic disease.

Technical considerations

Many abnormalities are accurately characterized by a combination of intermediate-weighted MR images without fat suppression and STIR (Short Tau Inversion Recovery) or T2-weighted MR images with fat suppression. In current practice, this is frequently achieved with the use of two-dimensional (2D) turbo spin echo (TSE) pulse sequences. 2D MR images can be acquired with a high in-plane spatial resolution, e.g. with a pixel size of 0.5 x 0.5 mm^2; however, in order to achieve a sufficient amount of MR signal, a slice thickness of 2-4 mm is required, which together with slice gaps generates partial volume effects. Owing to the inability for multiplanar reformations due to anisotropic voxel size, images in axial, sagittal and coronal orientation have to be acquired separately, which can be a time consuming process.

In contrast to 2D TSE, three-dimensional (3D) TSE using Sampling Perfection with Application optimized Contrast using different flip angle Evolutions (SPACE) is based on volume excitation and therefore yields markedly more MR signal. Using 3D SPACE with a high number of phase-encoding steps in z-direction enables the calculation of substantially thinner slice partitions and the generation of 3D MRI data sets with isotropic voxels size.

Such isotropic data sets with sufficiently small voxel size virtually eliminate partial volume effects and provide an opportunity for improved display of small anatomic detail. In addition, virtually any imaging plane can be reformatted from single parent data sets (Fig. 1), including standard axial, sagittal and coronal MR images, as well as oblique and curved planar reformations and 3D volume rendered MR images.

While this concept has been proven to be feasible with a diagnostic accuracy equal to or better than 2D TSE MRI [1-3], current 3D TSE techniques may be limited by low contrast-to-noise ratios (CNR), which could lead to limited conspicuity of cartilage and fluid [4], and image blur related to T2-decay during long echo trains and overall long acquisition times [5].

In order to increase the speed of 3D TSE image acquisition, one-dimensional parallel imaging techniques have been successfully applied, which reduces imaging time by undersampling in one phase encoding direction. Acceleration of 3D TSE, however, has typically been limited to a factor of 2, as higher unidirectional acceleration factors cause degradation of image

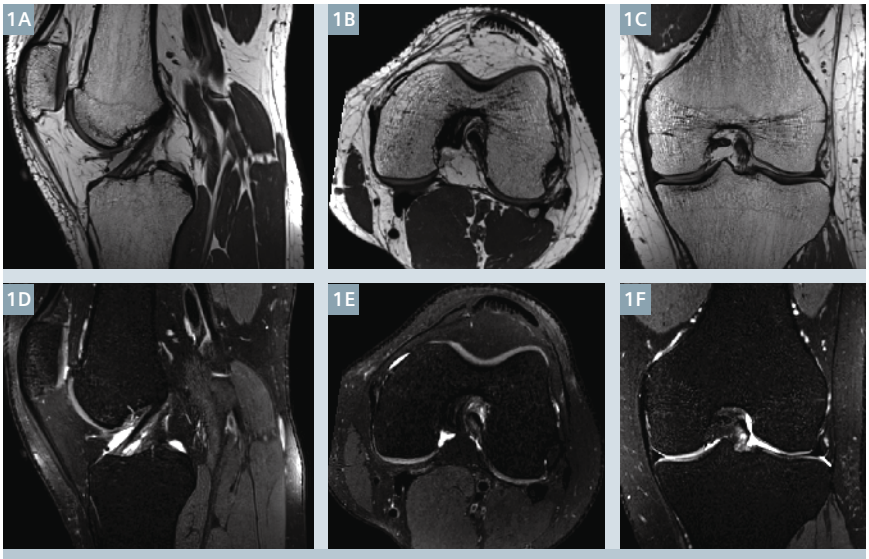

1 Normal left knee of a 37-year-old healthy man. Sagittal isotropic 0.5 mm intermediate-weighted and 0.6 mm T2 SPAIR-weighted 3D CAIPIRINHA SPACE source MR images **(1A and D)** with standard axial **(1B and E)** and coronal **(1C and F)** reformats.

quality through the occurrence of aliasing artifacts [6].

The CAIPIRINHA (Controlled Aliasing In Parallel Imaging Results IN Higher Acceleration) sampling pattern enables two-dimensional parallel imaging acceleration in both phase and partition encoding directions which substantially reduces aliasing artifacts and image noise through an optimized use of coil sensitivities [7, 8]. Multiple studies have shown the improved image quality and higher signal-to-noise ratios of gradient echo MR imaging techniques utilizing CAIPIRINHA when compared to standard parallel imaging technique such as GRAPPA [9].

CAIPIRINHA SPACE[1] is a new generation 3D TSE pulse sequence that enables high quality 3D TSE data acquisition with acceleration factors of 4 and similar or better image quality than conventional 3D SPACE and conventional 2D TSE sequences [10]. The high parallel imaging acceleration afforded by CAIPIRINHA enables the acquisition of high-resolution isotropic data sets with high signal and contrast-to-noise ratios that permit T1-, intermediate- and T2-weighted image contrasts without or with homogenous SPAIR (SPectrally Adiabatic Inversion Recovery) fat suppression. The 4-fold acceleration substantially reduces the time required for data acquisition and enables isotropic, high spatial resolution 3D MRI protocols for comprehensive evaluation of a multitude of musculoskeletal applications.

[1] WIP, CAIPIRINHA SPACE is currently under development and is not for sale in the US and in other countries. Its future availability cannot be ensured.

Clinical applications

The following clinical cases illustrate the application of a rapid high-resolution 3D CAIPIRINHA SPACE pulse sequence protocol for the evaluation of a variety of musculoskeletal conditions in adult and pediatric[2] patients. The 10-minute isotropic 3D CAIPIRINHA SPACE protocol consisted of intermediate-weighted MR images without fat suppression and T2-weighted MR images with fat suppression with parameter details given in Table 1. All studies were performed on a state-of-the-art 3-Tesla MR imaging system (MAGNETOM Skyra, Siemens Healthcare, Erlangen, Germany) with multi-channel surface coils, such as a 15-channel transmit/receive knee coil (QED, Mayfield Village, OH, USA), 18-channel body matrix and 16-channel ankle and foot receive-only coil (Siemens Healthcare).

Physeal bars

Physeal bars are due to a premature focal physeal arrest and cause interruptions of normal growth plate due to formation of a bony or fibrous bridge between the epiphysis and metaphysis. They can occur when there is contact between epiphysis and metaphysis due to damage to the physeal cartilage layers or displacement through a fracture. Physeal bars appear more commonly in the lower extremity than upper extremity and are common in the proximal tibia [11].

MRI is the method of choice for evaluation of physeal bars. MR imaging can accurately define the size and location and differentiate cartilaginous, fibrous and osseous components. Early fibrous bars appear as low signal intensity structures on intermediate-weighted MR images, while osseous physeal bars contain bone marrow and thus appear as hyperintense bridges between the epiphyseal and metaphyseal marrow on intermediate-weighted MR images that shows signal drop-out with fat suppression. Cartilaginous contents follow the characteristics of physeal cartilage and present with intermediate signal intensity on intermediate-weighted MR images and high signal intensity on fat-suppressed T2-weighted MR images.

Treatment strategies vary by site and type of growth arrest. For example, if at least 2 years or 2 cm of growth is predicted and the bar is <50% of the physeal area, then bar excision is recommended. If the bar involves more than 50% of physeal surface, completion of the arrest with an epiphysiodesis may be indicated [12].

[2] MR scanning has not been established as safe for imaging fetuses and infants less than two years of age. The responsible physician must evaluate the benefits of the MR examination compared to those of other imaging procedures.

Parameters	Intermediate-weighted 3D CAIPIRINHA SPACE	T2-SPAIR 3D CAIPIRINHA SPACE
Orientation	Sagittal	Sagittal
Repetition time (ms)	900	1100
Echo time (ms)	28	110
Echo train length	52	44
Receiver bandwidth (Hz/pixel)	422	399
Field-of-view (mm)	160 x 160	160 x 160
Voxel dimensions (mm)	0.5 x 0.5 x 0.5	0.63 x 0.63 x 0.63
Number of slices	240	190
In-plane frequency encoding direction	Anterior to posterior	Anterior to posterior
Acquisition time	5 min	5 min

Table 1: 10-minute 3D CAIPIRINHA SPACE isotropic orthopedic MR imaging protocol.

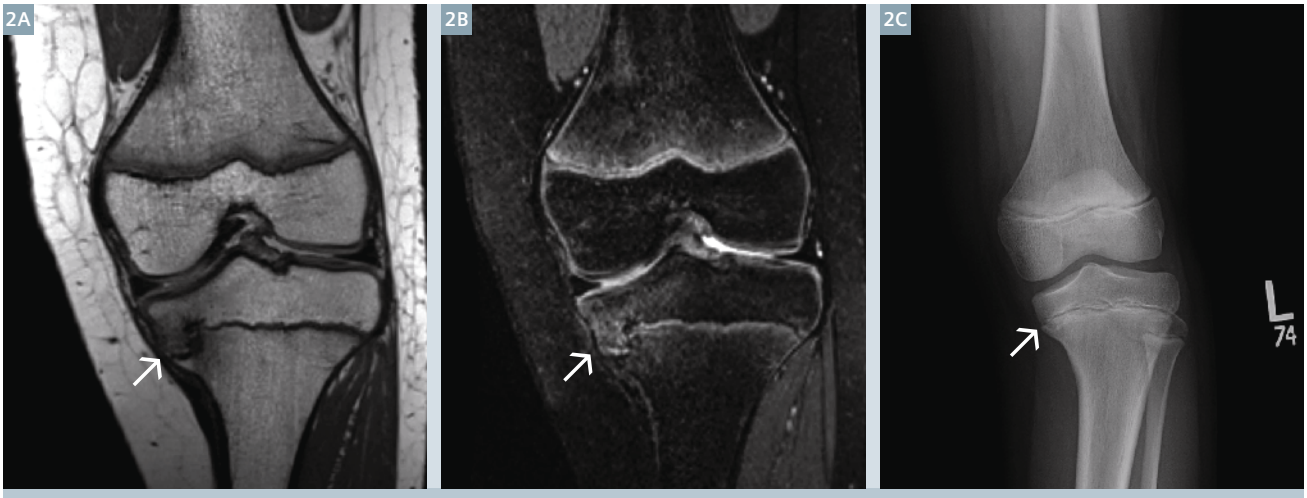

2 9-year-old girl with left knee pain and subtle deformity of the left proximal tibia. Coronal reformats of isotropic 0.5 mm intermediate-weighted **(2A)** and 0.6 mm T2 SPAIR-weighted **(2B)** 3D CAIPIRINHA SPACE MR images show a physeal bar (white arrows) across the medial aspect of the proximal tibial physis with mature bone marrow signal and mild edema pattern. Larger field-of-view antero-posterior radiograph **(2C)** shows mild left tibia vara deformity (Blount disease).

Bucket handle-type meniscal tear

Bucket handle meniscal tears are uncommon but characteristic vertical longitudinal tears that typically occur after a traumatic event; and in 80% of cases, involve the medial meniscus. The torn central meniscal fragment is often displaced towards the center of the joint, which can cause pain and locking symptoms. Bucket handle meniscal tears are frequently associated with anterior cruciate ligament (ACL) injuries [13].

On MR imaging, the double posterior cruciate ligament (PCL) sign is highly specific (98-100%) for the diagnosis of a displaced bucket handle tear [14]. A double PCL sign appears on sagittally oriented MR images when the medial meniscal tear displaces centrally so that it comes to locate anteroinferior to the PCL mimicking a second, smaller PCL. Rarely, a displaced lateral meniscus bucket handle tear may create a double PCL sign, which is often associated with a torn ACL. Careful MR imaging evaluation allows to differentiate the double PCL sign from accessory meniscofemoral and medial oblique meniscomeniscal ligaments. Other MR imaging signs can also be used to identify a bucket handle tear, such as absent bow tie, fragment within intercondylar notch, double anterior horn or flipped meniscus and disproportionally small posterior horn [15].

Historically, several treatments for bucket handle tears have been proposed such as arthroscopic subtotal meniscectomy and thermal shrinkage of posterolateral capsule. Current

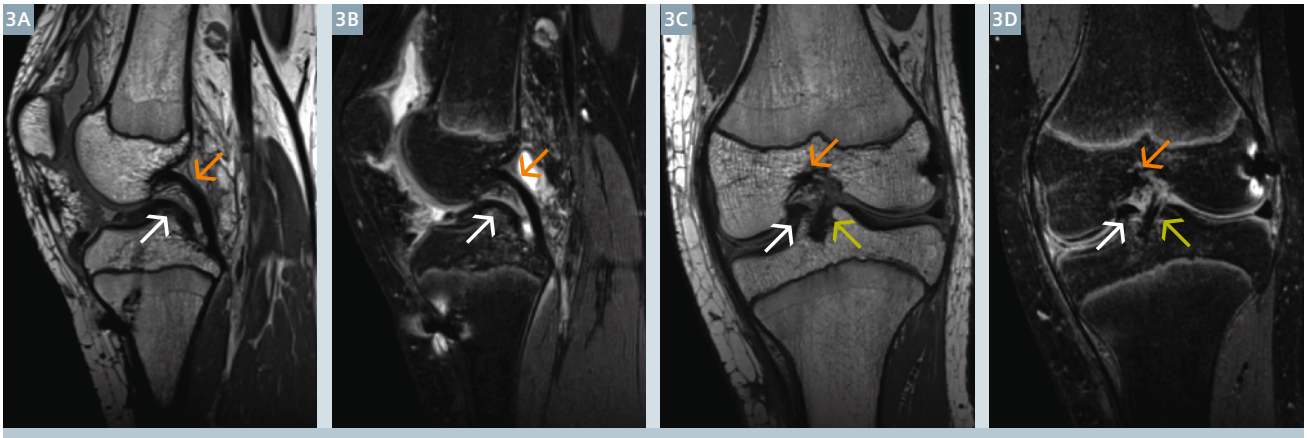

3 14-year-old teenager with left knee pain following healed anterior cruciate ligament reconstruction. Sagittal oblique isotropic 0.5 mm intermediate-weighted **(3A)** and 0.6 mm T2 SPAIR-weighted **(3B)** 3D CAIPIRINHA SPACE MR images with corresponding coronal reformats show a double PCL sign (3A and B, white arrows) of a bucket handle tear of the medial meniscus, created by displacement of the central meniscal fragment into the intercondylar notch. The posterior cruciate ligament (orange arrows) and the partially visualized anterior cruciate ligament graft (green arrows) are intact.

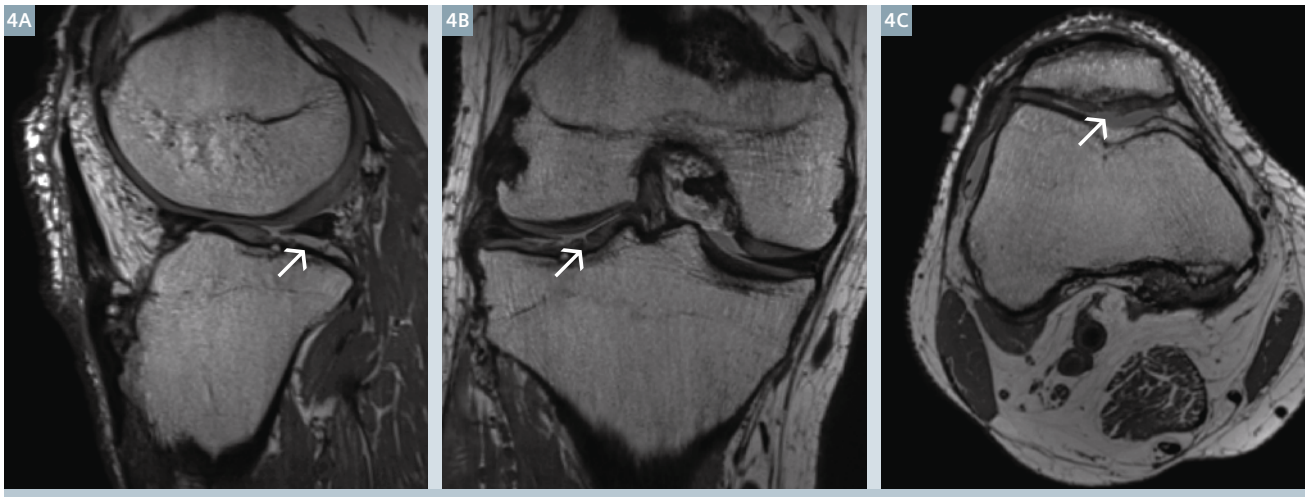

4 58-year-old man with right knee pain. Sagittal, coronal and axial reformats of an isotropic 0.5 mm intermediate-weighted 3D CAIPIRINHA SPACE MRI data set show full thickness cartilage loss over the posterior tibia plateau subjacent to the posterior third of the lateral meniscus (**4A**, arrow) as well as partial thickness cartilage defects and fissures of the articular cartilage of the central lateral tibia plateau (**4B**, arrow) and patella (**4C**, arrow). There is also a horizontal tear of the lateral meniscus.

treatment recommendations include meniscal preservation whenever possible with arthroscopic repair [16].

Cartilage defects

Loss of articular hyaline cartilage is the hallmark of degenerative osteoarthrosis and detectable by MR imaging before joint space narrowing occurs on radiographs. In clinical practice, cartilage defects may be graded with a modified Noyes or Outerbridge classification scheme [17]. The original Noyes score was based on arthroscopic findings, which was then modified for MR imaging findings. Modified Noyes score divides cartilage defect into 4 grades (Table 2).

Grades	Characteristics
Grade 0	Normal cartilage
Grade 1	Increased T2 signal intensity without loss of cartilage substance
Grade 2A	Superficial partial thickness cartilage loss of less than 50% of the total articular surface thickness
Grade 2B	Deep partial thickness cartilage loss equal to or more than 50% of total articular surface thickness
Grade 3	Full thickness cartilage loss with exposure of subchondral bone

Table 2: Modified Noyes classification for MR imaging grading of articular cartilage defects.

MRI is the modality of choice for assessment of cartilage damage. MR imaging techniques can evaluate both morphologic and compositional characteristics of articular cartilage. Morphological assessment of cartilage provides information about early cartilage degeneration as indicated by low or high signal intensity alterations, as well as substance defects such as fissuring, delamination, shear injuries and focal or diffuse partial and full thickness cartilage defects. Intermediate-weighted turbo spin echo pulse sequences with sufficiently high spatial resolution provide versatile and accurate morphological cartilage assessment due to their T2 sensitivity with good contrast between cartilage surface and the synovial fluid. Similar to 2D sequences, 3D sequences such as SPACE and Dual-Echo Steady State (DESS) provide high-contrast resolution between cartilage and synovial fluid for accurate assessment of cartilage integrity. Compositional MR imaging methods such as T2 mapping can be useful to identify early-stage degeneration [18]. Other compositional MR imaging methods include dGEMRIC, T1ρ, Sodium imaging and diffusion-weighted imaging.

Osteochondritis dissecans

Osteochondritis dissecans (OCD) describes the process of aseptic separation of the osseous component of an osteochondral fragment with gradual fragmentation of the articular surface. The condition typically occurs in active male teenagers and young adults. Patients may be asymptomatic, however, pain, joint locking and synovitis are common symptoms at the time of presentation. While the exact etiology is unknown, repetitive trauma and ischemia are suspected to play a major role. Approximately 75% of all cases occur in the femoral condyle, followed by the talus and the capitellum.

MRI is the diagnostic modality of choice for the characterization of osteochondritis dissecans, whereas radiography received a weak recommendation for the diagnosis of OCD by the American Academy of Orthopedic Surgeons (AAOS) due to the inability to visualize unossified

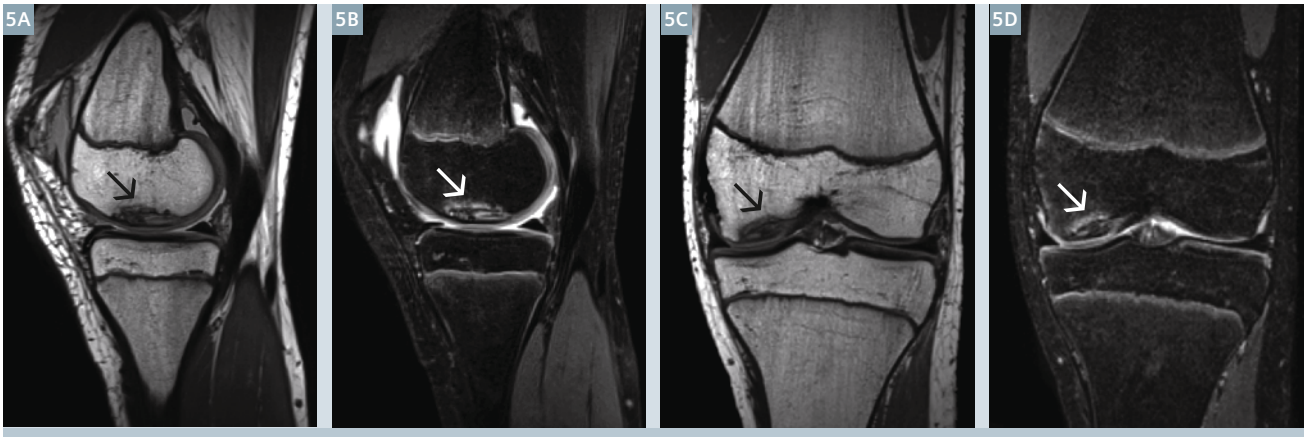

5 13-year-old teenager with left knee pain. Sagittal and coronal reformats of isotropic 0.5 mm intermediate-weighted **(5A and B)** and 0.6 mm T2 SPAIR-weighted **(5C and D)** 3D CAIPIRINHA SPACE MR images show a non-displaced osteochondritis dissecans lesion (arrows) along the inner margin of the medial femoral condyle. There are small cysts and a hyperintense rim along the host bone – fragment interface and a linear cartilage defect along the posterior margin.

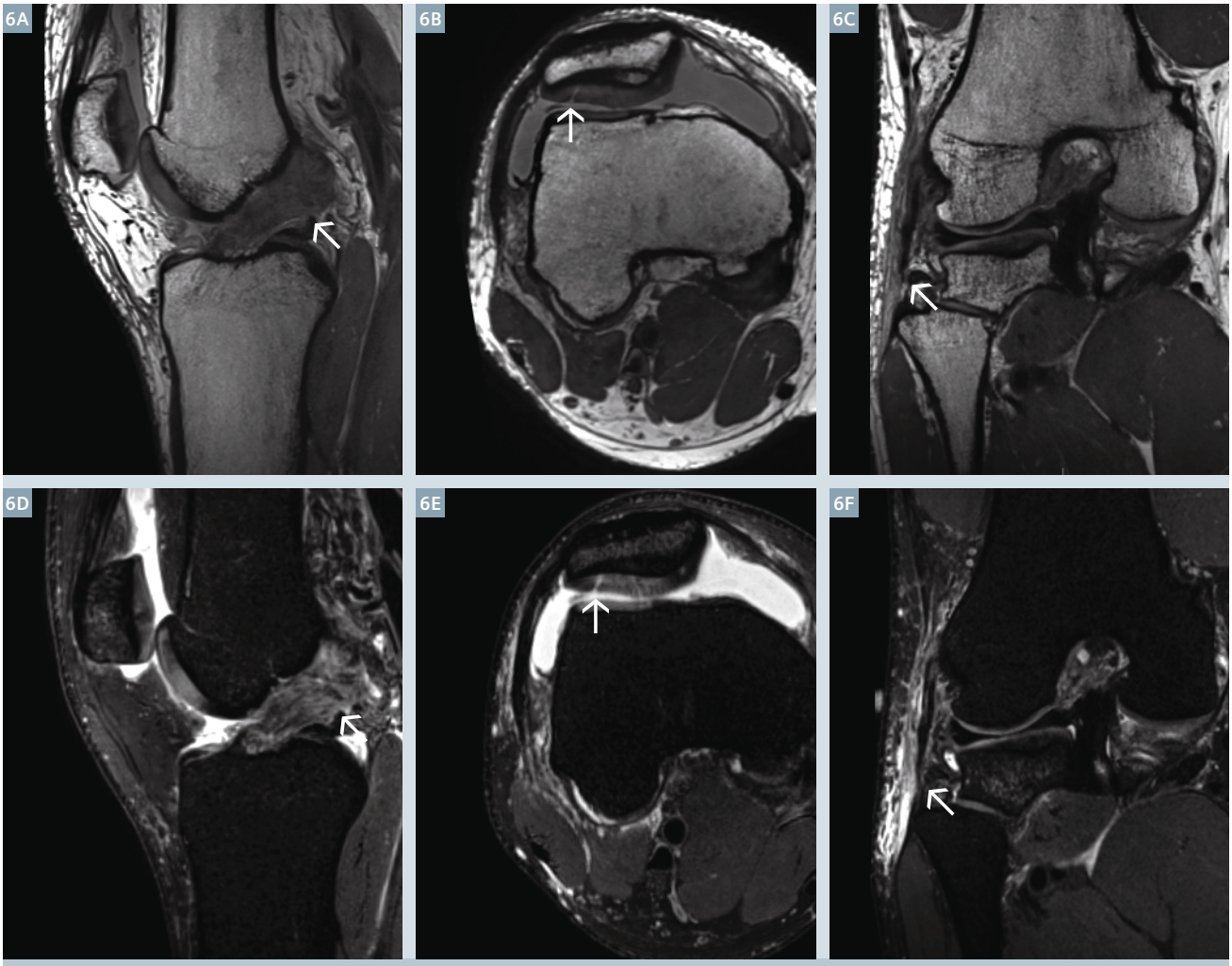

6 29-year-old man with history of recent American Football injury of the right knee. Sagittal oblique **(6A and D)**, axial **(6B and E)** and coronal oblique **(6C and F)** reformats of isotropic 0.5 mm intermediate-weighted and 0.6 mm T2 SPAIR-weighted 3D CAIPIRINHA SPACE MR images show a high-grade partial thickness tear of the anterior cruciate (arrows, 6A and D), a full-thickness fissure of the patellar cartilage (arrows, 6B and E) and a partial thickness tear of the lateral collateral ligament near the insertion (arrows, 6C and F).

elements and inability to assess for signs of mechanical instability [19].

Several MR imaging findings may be used to predict the stability of an OCD lesion [20, 21]. In adults with OCD of the knee, a high T2 signal intensity rim and cysts along the host bone – fragment interface, a high T2 signal intensity fracture line extending through the articular cartilage overlying an OCD lesion, and a fluid-filled osteochondral defect are signs of instability. In the pediatric population, a high T2 signal intensity rim or cysts surrounding the OCD lesion may be present in surgically stable OCD lesions; however, multiple cysts and a single cyst with a diameter greater than 5 mm have a high specificity for instability.

Anterior cruciate ligament tears

The anterior cruciate ligament (ACL) is the major restraint to anterior translation of the tibia relative to femur. It also provides restraint to rotatory forces. While one might assume that these injuries occur from contact mechanisms, ACL tears are more commonly non-contact injuries. Authors have described the pivot shift mechanism, which occurs when a combined valgus and axial force is exerted on the flexed knee with quadriceps loading, anterior tibial translation and external rotation of femur [22]. The combination of varus force with internal rotation of tibia and hyperextension of the knee joint may also cause ACL tears.

MRI is the reference standard for the imaging diagnosis of anterior cruciate ligament tears with sensitivity of 83%-95% and specificity of 95%-100% [23]. Depending on the extent of injury, MRI might show a focal discontinuity of the ACL, diffuse or focally abnormal signal intensity, abnormal bowing or non-visualization of the ligament. A major indication of MRI in the presence of an ACL injury is the evaluation for concomitant injuries, such as the collateral ligaments, menisci or articular cartilage. Fat suppressed, fluid sensitive MR images often show a pivot-shift-type osseous bone marrow edema contusion pattern at the posterolateral tibial plateau or condylopatellar sulcus at the lateral femoral condyle [23]. Chronically remodeled, complete ACL tears may demonstrate different patterns of scarring of the torn ligament remnants [24]. The most common injury pattern of partial ACL tears is a complete tear of anteromedial bundle with either an intact or partially torn posterolateral bundle [25].

Surgical treatment depends on the grade of injury and joint stability. Single bundle or double bundle ACL reconstructions may be performed with auto- or allografts. MRI has been shown to be accurate in identifying complete graft tears [26].

Medial collateral ligament tears

The superficial medial collateral ligament (MCL) provides the primary restraint to valgus loads, external rotation of the tibia, and anterior tibial translation when the anterior cruciate ligament is injured. The deep medial collateral ligament and the posterior oblique ligament provide additional stability to the medial knee joint and posteromedial corner. The medial collateral ligament is among the most frequently injured ligamentous structures of the knee with an annual incidence for injury between 0.24 and 7.3 per 1000 individuals [27].

Causes of medial collateral ligament injuries include direct valgus forces aimed at the knee, non-contact, or overuse injuries. The degree of injury and stability may be graded by the degree of medial joint line opening into grade 1 (<5 mm of medial joint line opening), grade 2 (5 to 10 mm) and grade 3 (>10 mm). MR imaging may be used to additionally grade the tear similar to the O'Donoghue classification (Table 3); however, it

Grading	Ligamentous Integrity	O'Donoghue classification	MRI classification
Grade 1	Interstitial injury	Structurally intact	Signal hyperintensity of the ligament without visualization of disrupted fibers
Grade 2	Partial thickness tear	Incomplete ligament tear, no valgus laxity	Disrupted and intact fibers
Grade 3	Full thickness tear	Complete ligament tear, valgus laxity	Disruption of all fibers

Table 3: MR grading of MCL tears.

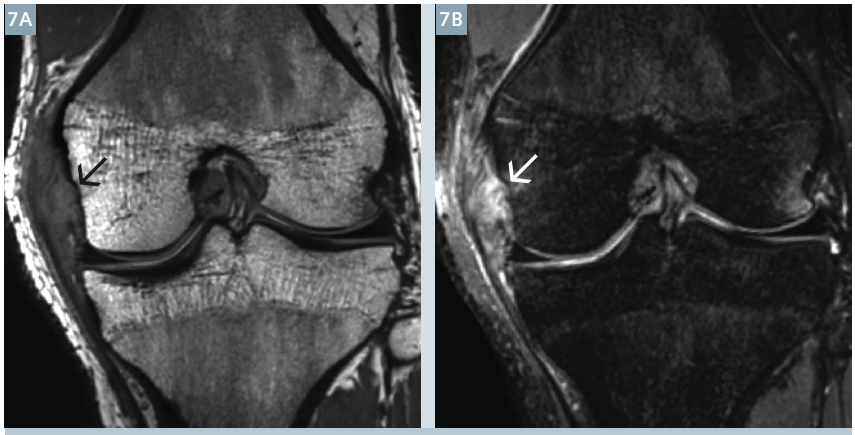

7 16-year-old teenager with recent trauma to the left knee during a soccer game. Coronal reformats of isotropic 0.5 mm intermediate-weighted **(7A)** and 0.6 mm T2 SPAIR-weighted **(7B)** 3D CAIPIRINHA SPACE MR images show a high-grade partial thickness tear (arrows) of the femoral origins of the superficial and deep medial collateral ligament.

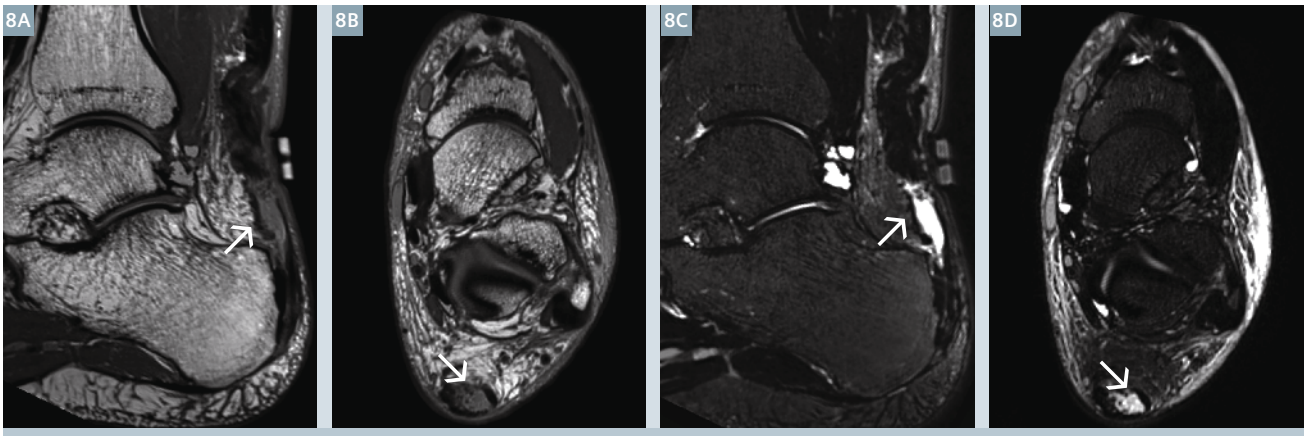

8 43-year-old man with recent ankle trauma and limited plantar flexion. Sagittal **(8A and C)** and axial **(8B and D)** reformats of isotropic 0.5 mm intermediate-weighted and 0.6 mm T2 SPAIR-weighted 3D CAIPIRINHA SPACE MR images show a complete distal midsubstance tear (arrows) of the degenerated Achilles tendon with retraction and gap formation.

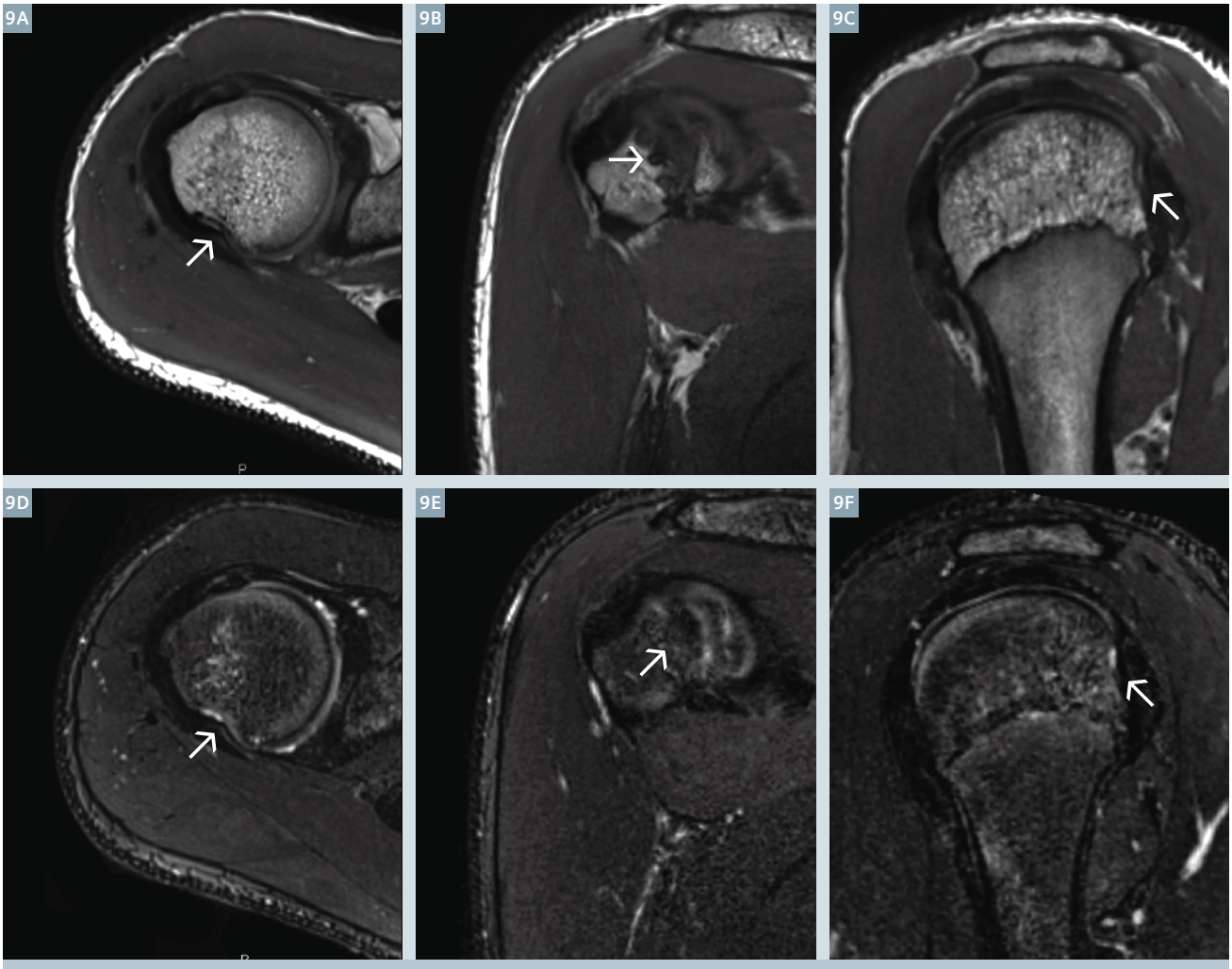

9 17-year-old boy with recent glenohumeral translation event during a Lacrosse game. Axial **(9A and D)**, coronal oblique **(9B and E)** and sagittal oblique **(9C and F)** reformats of isotropic 0.6 mm intermediate-weighted and 0.7 mm T2 SPAIR-weighted 3D CAIPIRINHA SPACE MR images show an acute Hill-Sachs fracture deformity (arrows) along the posterosuperior humeral head.

may be most helpful in the evaluation of tears associated with additional internal knee injuries. Depending on the severity, anterior cruciate ligament tears may be present in 20-78% of cases, medial meniscus tear in up to 55%, and extensor mechanism tears in up to 21%.

Conservative management and bracing has been advocated as primary method of treatment for low-grade injuries due to intrinsic healing capacity of the MCL, while surgical repair was reserved for grade III injuries, especially in athletes. However, recent studies have shown that a repair of the MCL might improve valgus stability in general population and thus, should be evaluated based on chronicity and extent of MCL injury along with appropriate patient selection [28].

Achilles tendon tears

The Achilles tendon is the most frequently injured tendon of the body. This tendon rupture occurs mostly in younger patients, predominantly male, and is typically sports-related. Physical activities that impart intermittent, but repetitive stress to the tendon without time given to adapt may lead to spontaneous rupture [29]. Other predisposing factors include intratendinous steroid injections, diabetes mellitus, use of fluoroquinolones and gout. Achilles tendon tears are often non-insertional, mid-substance ruptures, which is a region of relative hypovascularity located 2-6 cm proximal to insertion site.

MR imaging is highly accurate for the diagnosis of Achilles tendon rupture, which can be partial or complete. MR imaging shows a full thickness tear as a complete tendinous gap filled with edema or blood along with retraction ends, whereas a partial tear may be shown as longitudinal and transversal tendon substance defects that are hyperintense on intermediate-weighted and T2-weighted MR images. Timely diagnosis is important for optimal treatment outcome as delays are associated with poor outcomes such as weak plantar flexion and inability to run [30].

Glenohumeral translation

The Hill-Sachs lesion was first described by Hill and Sachs in 1940 as a "groove defect of the posterolateral humeral head" [31]. The Hill-Sachs lesion represents an impaction fracture of the posterosuperior or posterolateral humeral head and typically occurs when the humeral head impacts against the anteroinferior glenoid rim during an anteroinferior glenohumeral translation event [32, 33]. The lesion is acutely painful and may trigger recurring dislocation or subluxation as the groove defect serves as a lever, facilitating dislocation when the joint is extended and externally rotated. Hill-Sachs lesions are often associated with Bankart and Bankart-variant lesions of the anteroinferior glenoid labrum. MRI often shows a region of typically wedge shaped Hill-Sachs defect in the posterosuperior humeral head, which is accompanied with bone marrow edema pattern in the acute phase.

Developmental dysplasia of the hip

Developmental dysplasia of the hip (DDH) describes a range of deformities of the femoral head and acetabulum that are associated with dysfunction and pain and may lead to subluxation, instability and frank dislocation. Early detection is important, as treatment is more effective in infancy and becomes increasingly difficult at later stages with increasing risk of long term disability [34].

The condition may be diagnosed by physical examination using a variety of tests, such as the Barlow or Ortolani procedures. Ultrasound is considered a good diagnostic tool but, lately, its role in screening has been debated [35]. While MRI does not play a major role in screening for DDH [36], its major utility lies in the evaluation of the degree of cartilage loss as well as the assessment of joint congruity and condition of growth cartilage and ossification centers [37]. MR imaging is also useful for the assessment following surgical joint relocation and application of spica cast.

In summary, 3D CAIPIRINHA SPACE is a new technique that enables the isotropic acquisition of high-quality 3D data sets for efficient and comprehensive MRI of joints.

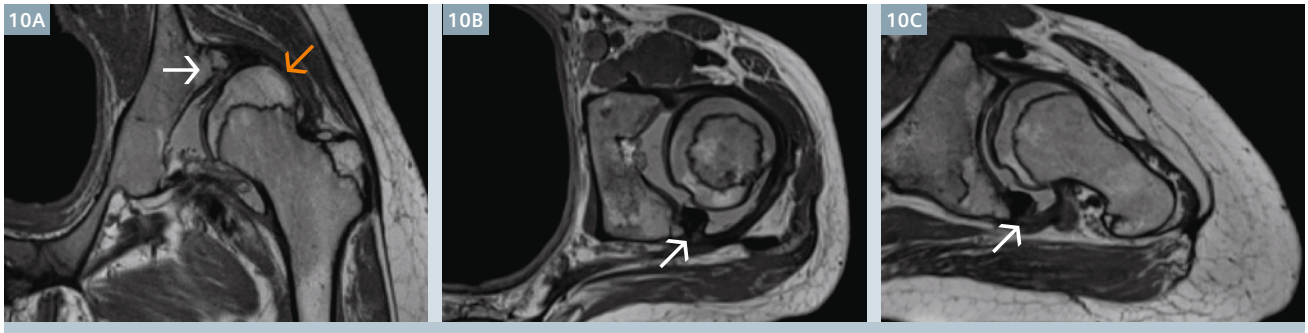

10 28-year-old woman with history of developmental dysplasia of the left hip. Coronal oblique **(10A)**, axial **(10B)** and axial oblique **(10C)** reformats of isotropic 0.7 mm intermediate-weighted 3D CAIPIRINHA SPACE MR images show a dysplastic acetabulum with deficient lateral femoral head coverage (10A, white arrow) as well as lateral subluxation of the deformed femoral head (10A, orange arrow). There is moderate synovitis and hypertrophy of the degenerated acetabular labrum (10B and C, arrows).

References

1 M. Notohamiprodjo, A. Horng, M.F. Pietschmann, et al. MRI of the knee at 3 T: first clinical results with an isotropic PDfs-weighted 3D-FSE-sequence Investigative Radiology, 44 (9) (2009), pp. 585–597.

2 Notohamiprodjo M, Horng A, Kuschel B, Paul D, Li G, Raya JG, Reiser MF, Glaser C. 3D-imaging of the knee with an optimized 3D-FSE-sequence and a 15-channel knee-coil. Eur J Radiol. 2012 Nov;81(11):3441-9.

3 Notohamiprodjo M, Kuschel B, Horng A, Paul D, Baer P, Li G, Garcia del Olmo JM, Reiser MF, Glaser C. 3D-MRI of the ankle with optimized 3D-SPACE. Invest Radiol. 2012 Apr;47(4):231-9.

4 K.J. Stevens, R.F. Busse, E. Han, et al. Ankle: isotropic MR imaging with 3D-FSE-cube—initial experience in healthy volunteers Radiology, 249 (3) (2008), pp. 1026–1033.

5 R. Kijowski, K.W. Davis, M.A. Woods, et al. Knee joint: comprehensive assessment with 3D isotropic resolution fast spin-echo MR imaging—diagnostic performance compared with that of conventional MR imaging at 3.0 T Radiology, 252 (2) (2009), pp. 486–495.

6 Breuer FA, Blaimer M, Mueller MF, Griswold MA, Jakob PM. CAIPIRINHA-Revisited. MAGNETOM Flash 2015;3(63):8-15.

7 Breuer FA, Blaimer M, Mueller MF, et al. Controlled aliasing in volumetric parallel imaging (2D CAIPIRINHA). Magn Reson Med 2006; 55:549-556.

8 Horger W, Kiefer B. Fat Suppression Techniques –a Short Overview. MAGNETOM Flash 2011;1(46):56-59.

9 Wright KL, Harrell MW, Jesberger JA, et al. Clinical evaluation of CAIPIRINHA: comparison against a GRAPPA standard. J Magn Reson Imaging 2014; 39:189-194.

10 Fritz J, Fritz B, Thawait GG, Meyer H, Gilson WD, Raithel E. Three-Dimensional CAIPIRINHA SPACE TSE for 5-Minute High-Resolution MRI of the Knee. Invest Radiol. 2016 Oct;51(10):609-17.

11 Khoshhal KI, Kiefer GN. Physeal bridge resection. J Am Acad Orthop Surg. 2005 Jan-Feb;13(1):47-58.

12 Gauger EM, Casnovsky LL, Gauger EJ, Bohn DC, Van Heest AE. Acquired Upper Extremity Growth Arrest. Orthopedics. 2016 Sep 29:1-9.

13 Boody BS, Omar IM, Hill JA. Displaced Medial and Lateral Bucket Handle Meniscal Tears With Intact ACL and PCL. Orthopedics. 2015 Aug;38(8):e738-41.

14 Camacho MA. The double posterior cruciate ligament sign. Radiology. 2004 Nov;233(2):503-4.

15 Nguyen JC, De Smet AA, Graf BK, Rosas HG. MR imaging-based diagnosis and classification of meniscal tears. Radiographics. 2014 Jul-Aug;34(4):981-99.

16 Ahn JH, Kim KI, Wang JH, Kyung BS, Seo MC, Lee SH. Arthroscopic repair of bucket-handle tears of the lateral meniscus. Knee Surg Sports Traumatol Arthrosc. 2015 Jan;23(1):205-10.

17 Crema MD, Roemer FW, Marra MD, Burstein D, Gold GE, Eckstein F, Baum T, Mosher TJ, Carrino JA, Guermazi A. Articular cartilage in the knee: current MR imaging techniques and applications in clinical practice and research. Radiographics. 2011 Jan-Feb;31(1):37-61.

18 Dunn TC, Lu Y, Jin H, Ries MD, Majumdar S. T2 relaxation time of cartilage at MR imaging: comparison with severity of knee osteoarthritis. Radiology. 2004 Aug;232(2):592-8.

19 Zbojniewicz AM, Laor T. Imaging of osteochondritis dissecans. Clin Sports Med. 2014 Apr;33(2):221-50.

20 Kijowski R, Blankenbaker DG, Shinki K, Fine JP, Graf BK, De Smet AA. Juvenile versus adult osteochondritis dissecans of the knee: appropriate MR imaging criteria for instability. Radiology. 2008 Aug;248(2):571-8.

21 Samora WP, Chevillet J, Adler B, Young GS, Klingele KE. Juvenile osteochondritis dissecans of the knee: predictors of lesion stability. J Pediatr Orthop. 2012 Jan-Feb;32(1):1-4.

22 Quatman CE, Quatman-Yates CC, Hewett TE. A 'plane' explanation of anterior cruciate ligament injury mechanisms: a systematic review. Sports Med. 2010 Sep 1;40(9):729-46.

23 Naraghi A, White LM. MR imaging of cruciate ligaments. Magn Reson Imaging Clin N Am. 2014 Nov;22(4):557-80.

24 Nakase J, Toratani T, Kosaka M, Ohashi Y, Tsuchiya H. Roles of ACL remnants in knee stability. Knee Surg Sports Traumatol Arthrosc. 2013 Sep;21(9):2101-6.

25 Ng AW, Griffith JF, Hung EH, Law KY, Yung PS. MRI diagnosis of ACL bundle tears: value of oblique axial imaging. Skeletal Radiol. 2013 Feb;42(2):209-17.

26 Horton LK, Jacobson JA, Lin J, Hayes CW. MR imaging of anterior cruciate ligament reconstruction graft. AJR Am J Roentgenol. 2000 Oct;175(4):1091-7.

27 Roach CJ, Haley CA, Cameron KL, Pallis M, Svoboda SJ, Owens BD. The epidemiology of medial collateral ligament sprains in young athletes. Am J Sports Med. 2014 May;42(5):1103-9.

28 Long JM, Waterman BR. Surgical Repair of Medial Collateral Ligament and Posteromedial Corner Injuries of the Knee: A Systematic Review. Arthroscopy. 2015 Nov;31(11):2249-55.

29 Schweitzer ME, Karasick D. MR imaging of disorders of the Achilles tendon. AJR Am J Roentgenol. 2000 Sep;175(3):613-25.

30 Singh D. Acute Achilles tendon rupture. BMJ. 2015 Oct 22;351:h4722.

31 Hill HA, Sachs MD. The grooved defect of the humeral head: a frequently unrecognized complication of dislocations of the shoulder joint. Radiology. 1940;35: 690–700.

32 Richards RD, Sartoris DJ, Pathria MN, Resnick D. Hill-Sachs lesion and normal humeral groove: MR imaging features allowing their differentiation. Radiology. 1994 Mar;190(3):665-8.

33 Demehri S, Hafezi-Nejad N, Fishman EK. Advanced imaging of glenohumeral instability: the role of MRI and MDCT in providing what clinicians need to know. Emerg Radiol. 2016 Aug 13. [Epub ahead of print].

34 Kotlarsky P, Haber R, Bialik V, Eidelman M. Developmental dysplasia of the hip: What has changed in the last 20 years? World J Orthop. 2015 Dec 18;6(11):886-901.

35 US Preventive Services Task Force. "Screening for Developmental Dysplasia of the Hip: Recommendation Statement." PEDIATRICS 117, no. 3 (3, 2006): 898-902. doi:10.1542/peds.2005-1995.

36 Karmazyn BK, Gunderman RB, Coley BD, et al. ACR Appropriateness Criteria on developmental dysplasia of the hip: child. J Am Coll Radiol 2009;6(8):551–557.

37 Rosenbaum DG, Servaes S, Bogner EA, Jaramillo D, Mintz DN. MR Imaging in Postreduction Assessment of Developmental Dysplasia of the Hip: Goals and Obstacles. Radiographics. 2016 May-Jun;36(3):840-54.

Contact

Jan Fritz, M.D., P.D., D.A.B.R.
Director of Interventional MR Imaging
Associate Director MSK Fellowship
Assistant Professor of Radiology and Radiological Sciences
Johns Hopkins University School of Medicine
Russell H. Morgan Department of Radiology and Radiological Science
Musculoskeletal Radiology
601 N. Caroline Street, JHOC 3140A
Baltimore, MD 21287, USA
jfritz9@jhmi.edu